Bridge–Assisted Ultrafast Interfacial Electron Transfer to Nanocrystalline SnO2 Thin Films

5 **AUTHORS**, INCLUDING:

Debra L Mohler
James Madison University
47 PUBLICATIONS **1,000** CITATIONS

Tianquan Lian
Emory University
159 PUBLICATIONS **7,194** CITATIONS

Bridge-Assisted Ultrafast Interfacial Electron Transfer to Nanocrystalline SnO$_2$ Thin Films

Neil A. Anderson, Xin Ai, Daitao Chen, Debra L. Mohler,* and Tianquan Lian*

Department of Chemistry, Emory University, Atlanta, Georgia 30322

Received: May 24, 2003; In Final Form: October 10, 2003

The electron-transfer rate from methylene-bridged molecular adsorbates to SnO$_2$ semiconductor nanocrystalline film was systematically investigated for short bridge lengths. The synthesized sensitizers were the homologues of Re(CO)$_3$Cl(dcbpy) [dcbpy = 4,4′-dicarboxy-2,2′-bipyridine] (ReC*n*A) with methylene units (CH$_2$)$_n$ (n = 1−5) inserted between the bipyridine rings and the carboxylate anchoring groups. Use of femtosecond infrared spectroscopy provided the time resolution necessary to study the ultrafast electron transfer that occurs over these very short bridges. Electron injection is unambiguously observed by signals arising from both the injected electron and the CO stretching mode of the oxidized molecule. All dyes exhibited nonexponential electron injection. The kinetic traces for the different spacers can be superimposed on each other by scaling their time axes, which allows a quantitative comparison of these nonexponential injection rates. This comparison revealed an exponential decrease of injection rate with bridge length for $3 \le n \le 5$ with a decay constant (β) of 1.0 per CH$_2$ unit. Deviation from the exponential dependence was observed for n = 1 or 2. The applicability of the time-scaling method also implies a rate distribution that is nominally independent of bridge length for all of the investigated samples.

Introduction

Bridge-assisted electron transfer (ET) is a phenomenon of central importance to chemistry,[1] biology,[2−5] and molecular electronics.[6−10] Generally, the bridge-length dependence of ET rate from a molecular adsorbate to a metal or semiconductor electrode has been extensively studied for long bridges,[10−21] but the behavior with short bridges is not well understood.[22−24] In this case, interfacial electron transfer can occur on the picosecond time scale, a measurement regime that has proven difficult for conventional electrochemistry-based techniques. Such ultrafast processes have become increasingly important in molecular electronics[6−10] and dye-sensitized solar cells.[25−27] High photon-to-current conversion in dye-sensitized solar cells is attributed to the efficient ultrafast photoinduced charge injection from the dye to the semiconductor[28−31] combined with slow back electron transfer.[32,33] Thus, the optimal control of the injection and recombination rates via molecular spacer design is a promising approach to improving cell performance.[34−38] Additionally, this strategy may provide the answer to the fundamental question of how bridge-assisted charge transfer between a molecular component and a metal or semiconductor electrode contributes to overall molecular conductance.[10,39]

Of the many molecular bridges examined so far,[10−21,40] the methylene spacer group (alkyl chain) is one of the most studied with many reports of the effect of alkyl chain length on interfacial electron transfer through alkanethiol monolayers on gold.[11,12,16,18−21,41,42] For eight or more methylene units ($n \ge 8$), the ET rate constant, k_{ET}, was shown to vary exponentially with n:

$$k_{ET} = k_{ET,n=0} \, e^{-\beta_n n} \tag{1}$$

where β_n is the exponential decay coefficient and $k_{ET,n=0}$ is the extrapolated value of the rate constant for n = 0. In the weak coupling nonadiabatic limit, the ET rate depends on the square of the electronic coupling strength between donor and acceptor, and the observed correlation can be attributed to the dependence of electronic coupling on n.[43−45]

For short bridge length, the relationship of electronic coupling to the number of spacer units and the dependence of rate on the coupling strength in the strong coupling limit are poorly understood. Theoretical studies predict the dependence of coupling on the number of spacers in short alkyl chains to deviate from exponential[43,46−49] and to oscillate between odd and even n.[50,51] This behavior is expected to be general for bridge-assisted electron-transfer processes.[43,44] Indeed, the odd−even effect in ET rates has been observed in some methylene-bridged molecular donor−acceptor complexes in solution[52] but not all.[53−56] For interfacial ET, this phenomenon is even less well understood. In a recent study of ET through short chain (n = 2−8) alkanethiol self-assembled monolayers (SAMs), the n dependence was found to level off at n = 2, which was attributed to the solvent viscosity dependence of ET in the adiabatic regime.[23] Similar reduction of distance dependence at even longer distance has also been observed for alkanethiol[12,40] and oligophenylenevinylene bridges.[22]

Most bridge-assisted interfacial ET rates have been determined by cyclic voltammetry and chronoamperometry in electrochemical cells with SAM-modified electrodes[11,12,16,18−21,23,41,42] While these techniques are useful for systems containing longer bridges that form well-ordered SAMs, the extension of current- or voltage-based approaches to shorter bridge length has proven difficult, with the exception of a novel laser-induced temperature jump technique.[12,22,40] In contrast, ultrafast spectroscopic techniques allow the direct measurement of bridge-dependent ET over short bridges[57,58] on a multi-femtosecond time scale.[59] More recently, transient absorption spectroscopy has been used to investigate ultrafast long distance electron transfer through a series of molecular tripods.[34−37]

* To whom correspondence should be addressed. E-mail addresses: tlian@emory.edu; dmohler@emory.edu.

SCHEME 1: Structures of the Re Dyes*[a]*

ReC0A	**1a**	n = 0
ReC1A	**1b**	n = 1
ReC2A	**1c**	n = 2
ReC3A	**1d**	n = 3
ReC4A	**1e**	n = 4
ReC5A	**1f**	n = 5
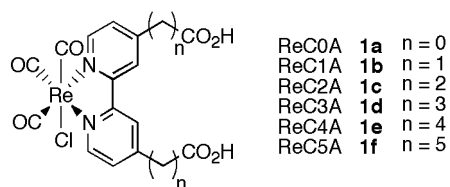
[a] Dyes with *n* = 1−5 methylene bridging groups between the bipyridine and the carboxylate binding group were studied.

Although such transient absorption based techniques are not easily applied to systems consisting of one monolayer of adsorbates on a flat electrode surface, extensive studies have demonstrated the excellent suitability of these methods to adsorbates on nanoparticles or nanocrystalline thin films because of their large surface area.[28−31,57,58,60−80]

Ultrafast infrared spectroscopy has provided valuable data on electron transfer from adsorbed molecules to semiconductor nanoparticles and nanocrystalline thin films[60,66,78,81] because it allows simultaneous observation of electrons injected into the semiconductor and changes in the vibrational spectrum of the adsorbate.[57,63,66,82] Here, we report the results of the ultrafast infrared spectroscopic investigation of electron injection from a rhenium complex to a SnO$_2$ nanocrystalline film as a function of bridge length. The structures of the adsorbates containing various alkyl bridge lengths are shown in Scheme 1. In the bridged dyes, the dcbpy ligand was modified with alkyl chains of *n* methylene groups between the bipyridine moiety and the carboxylate anchoring groups (ReC*n*A, *n* = 1, 2, 3, 4, 5), which bond to the Sn^{4+} sites in SnO$_2$ and adsorb the dye to the semiconductor nanoparticle.[83] In these complexes, excitation at 400 nm induces a transition to a singlet metal-to-ligand charge-transfer (^{1}MLCT) state, transferring electron density from a d orbital of the Re(I) metal center to a π^* orbital of the bipyridine ligand.[84,85] The conduction band edge of SnO$_2$ at pH 2 is $\sim$0 V vs SCE,[83] substantially lower in energy than the redox potential of the excited state of these dyes ($\sim$0.65 eV for ReC1A, **1a**),[57,84,86] resulting in energetically favorable electron transfer to SnO$_2$. Previously, the rates of bridge-assisted ET in a subset (*n* = 0, 1, 3) of the dyes on TiO$_2$ film were found to decrease with increasing *n*,[57] but a quantitative analysis of the dependence was hindered by the small set of molecules available and by differing energetics for ReC0A relative to the bridged dyes. By utilizing an expanded set of molecules, we can now systematically investigate bridge-length-dependent ultrafast interfacial ET.

Experimental Section

Synthesis of Rhenium Complexes. Detailed synthetic procedures and spectroscopic data for the Re(CO)$_3$Cl complexes **1a−e** and **3a−e** are given in the Supporting Information. Briefly, the preparation of the Re(CO)$_3$Cl complexes **1a−e** of the ester-

substituted bipyridine ligands **2a−e**[87] was accomplished (Scheme 2) in a manner similar to that reported for Re(CO)$_3$Cl(dcbpy).[88] Thus, each of the esters reacted with Re(CO)$_5$Cl in methanol at reflux to give good yields of the complexes **3a−e**, which were subsequently hydrolyzed in aqueous HCl to give the carboxylic acid-substituted complexes **1a−e**. Initially, the metal complexation step was attempted with the diacid-substituted bipyridine ligands; however, these conditions led to inseparable mixtures of the desired diacid-substituted rhenium complex with the corresponding mono- and diester analogues. This finding, in conjunction with the fact that the bipyridinediesters are the immediate precursors to the diacids,[87] suggested that the ester hydrolysis should be conducted after metal complex formation.

Preparation of Dye-Adsorbed Nanocrystalline Thin Films. Colloidal rutile SnO$_2$ was synthesized according to a published procedure.[89] Preparation of the transparent and relatively homogeneous SnO$_2$ films was described previously.[64] Films were sensitized by soaking in a methanol solution of dye for several hours. The sensitized films were then removed from the solution, rinsed with methanol to remove excess dye, then soaked in a pH 2 buffer for at least 4 h. During transient absorption experiments, the films were kept in contact with a small volume of the buffer and samples were moved continuously to avoid damage or photoproduct buildup. Dye absorption at the 400 nm pump wavelength was typically 0.3−0.4 OD.

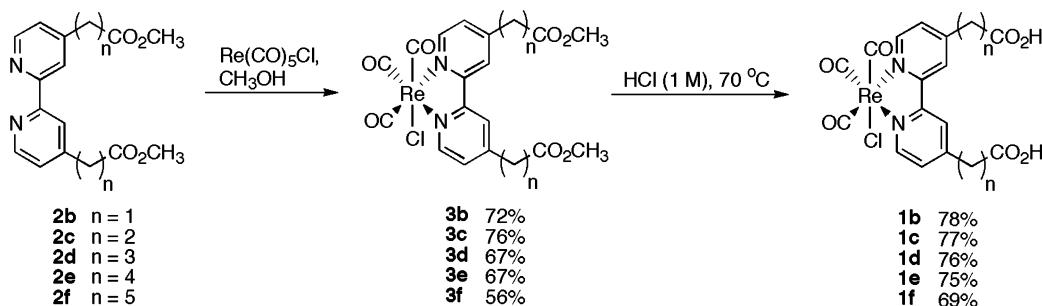**Ultrafast Infrared Transient Absorption Measurements.** The tunable infrared spectrometer used for these studies utilizes a 1 kHz regeneratively amplified Ti:sapphire laser system (800 nm, 100 fs, 900 μJ/pulse). Difference frequency generation from the signal and idler of an IR OPA produced the tunable mid-IR probe pulses, which had a $\sim$250 cm^{-1} bandwidth. Frequency doubling the laser fundamental provided the 400 nm pump beam. Details of the pump−probe setup have been previously reported.[63,82]

Experiments were carried out using $\sim$2 μJ of pump power at 400 nm with a spot size of 500 μm at the sample. The mid-IR probe beam was focused to 300 μm at the sample. After passing through the sample, the probe was then dispersed in a spectrometer and detected using a 32-element MCT array detector. The spectral resolution was 15 nm ($\sim$6 cm^{-1} at 2100 cm^{-1}). Zero time delay was defined and the instrument response was characterized utilizing a silicon wafer or CdS film, either of which gives an instantaneous absorption response to the pump beam. Typically, the instrument response at the sample was well characterized by a 200−250 fs fwhm Gaussian function.

Results

Demonstration and Observation of Charge Transfer. The stretching modes of the CO ligands exhibit strong absorption cross sections, an ideal characteristic for studies by ultrafast infrared spectroscopy. These vibrational modes are clearly
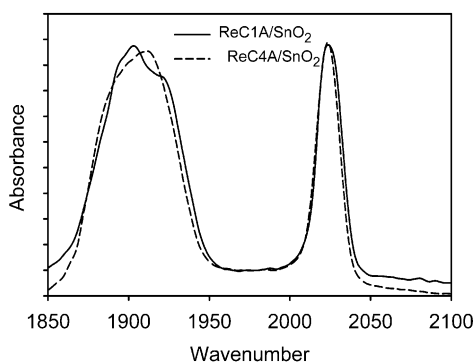
SCHEME 2

2b n = 1	
2c n = 2	
2d n = 3	
2e n = 4	
2f n = 5	

3b	72%
3c	76%
3d	67%
3e	67%
3f	56%

1b	78%
1c	77%
1d	76%
1e	75%
1f	69%

Bridge-Assisted Ultrafast Interfacial ET

J. Phys. Chem. B, Vol. 107, No. 51, 2003 **14233**

Figure 1. FTIR spectra of ReC1A (—) and ReC4A/SnO$_2$ (− − −) at pH 2 in the CO stretching region. All of the bridged dyes on SnO$_2$ at pH 2 exhibited virtually identical spectra in this region. The lower-energy peak at 1904 cm^{-1} is a superposition of two poorly resolved CO stretching modes, while the higher-energy peak at 2022 cm^{-1} corresponds to a single CO stretching mode.

shown in the FTIR spectra (Figure 1) of ReC1A and ReC4A on SnO$_2$ films at pH 2. The peak frequencies of 1904 and 2022 cm^{-1} are virtually identical for all dyes with $n \geq 1$ under these conditions. While the lower-energy peak is actually composed of two poorly resolved overlapping CO stretch modes, the higher energy peak originates from only one mode. Therefore, to avoid complications due to such overlap, the transient absorption spectra discussed herein focus on the highest-energy CO stretching mode for the dye electronic ground, excited, and oxidized states.

As shown in Figure 2a, the transient difference spectra for ReC1A/SnO$_2$ collected at several time delays all exhibit a broad absorption signal with narrower vibrational bands of the ReC1A dye superimposed. The broad signal maintains a relatively constant slope at all delay times, but the intensity increases with time delay. As a guide for each transient spectrum, an estimate of this signal is indicated. This signal arises from electrons injected into SnO$_2$, which exhibit steadily increasing absorption toward longer wavelengths starting at ∼4000 cm^{-1}.[64] Previous results showed a 15−20% slope for the electron signal within the spectral window of the present measurement,[64] which is largely consistent with the spectra in Figure 2a.

Evolution of the ReC1A vibrational peaks is shown more clearly upon subtraction of the electron signal from the raw spectra, giving the sensitizer-associated difference spectra shown in Figure 2b with offsets applied for clarity. The CO stretching modes observed following excitation of ReC1A on semiconductor nanoparticles have been assigned previously.[57,63] The photobleach (relative to the SnO$_2$ injected electron background) at 2025 cm^{-1} corresponds to the electronic ground state, consistent with its FTIR spectrum. New absorption peaks are observed at 2047 and 2092 cm^{-1} and correspond to the highest-energy CO stretch frequencies for the electronic excited-state and oxidized dye, respectively. The excited-state CO stretch is blue-shifted relative to the ground state because of the reduction of electron density at the Re center upon MLCT excitation. This effect diminishes the back-bonding from the metal to the π^* orbital of the CO ligand, strengthening the CO bond and increasing the stretching frequency.[90−93] Because of mixing between the bipyridine π^* orbitals and Re d orbitals, the oxidization of the molecule further reduces the charge density at the metal center, leading to even greater blue-shifting of the band in the oxidized dye.

Oxidation of ReC1A is clearly indicated in the transient spectra of Figure 2. At short delay times, the excited-state peak is large and the oxidized peak is not clearly observed. The
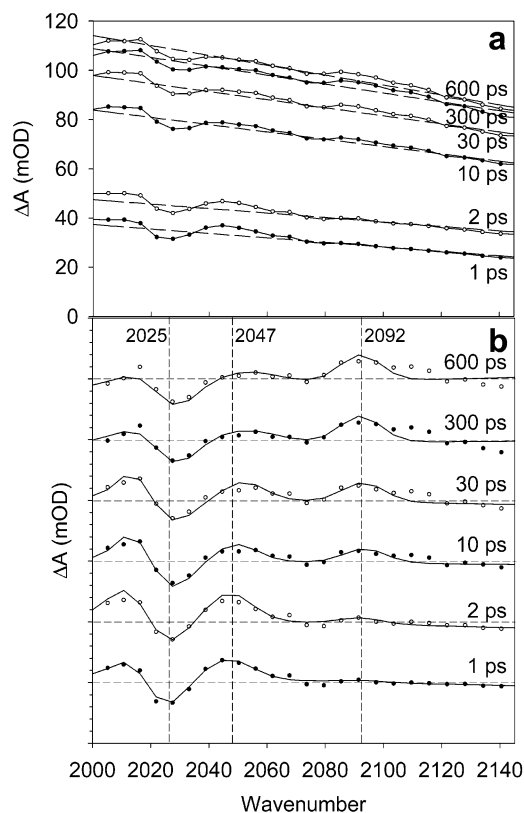

Figure 2. Transient spectral evolution (a) of ReC1A/SnO$_2$ at pH 2. A broad, sloped absorption signal increases with time and is attributed to electrons injected into SnO$_2$. The estimated injected electron signal for each time delay is shown by a dashed line. The electron signal underlies vibrational peaks from the ReC1A highest-energy CO stretch, shown more clearly in panel b. Panel b shows the transient dye spectra for ReC1A/SnO$_2$ obtained by taking the spectra of panel a and subtracting the electron signal to clearly show the spectral evolution of the dye. The spectra are on the same ΔA scale and are offset for clarity. The bleach (relative to the electron signal) at 2025 cm^{-1} corresponds to depopulation of the ReC1A electronic ground state after photoexcitation. It is observed immediately upon excitation and retains a qualitatively similar size at all time delays. The absorption peak at 2047 cm^{-1} is assigned to the highest-energy CO stretching mode in the dye excited state. This peak is strongest at early time delays and has nearly disappeared by 600 ps. The 2092 cm^{-1} absorption peak arises from the oxidized dye following electron transfer. It is not clearly observed at early time delays and increases with time.

excited-state peak decays with time, concurrent with growth of the oxidized peak. The excited state has virtually disappeared within 600 ps. Throughout all time delays, the size of the ground-state bleach remains reasonably constant, although a quantitative analysis of the bleach size is difficult because of overlapping absorptions. The excited-state decay without change in bleach size indicates that oxidization is the primary deactivation pathway for excited ReC1A on SnO$_2$. Similar spectra collected for each of the other bridged dyes on SnO$_2$ all exhibited an increase in the broad electron background absorption and decay of the excited-state peak, concomitant with growth of the oxidized peak. The spectra varied primarily in the rate of the evolution from the excited state to the oxidized form and in the rate of growth of the signal due to injected electrons.

In principle, the electron-transfer rate may be monitored using either the injected electron or oxidized molecule signal. However, some care must be exercised in using the injected electron trace, as demonstrated by our previous study of ReC0A on TiO$_2$. In that case, injection occurs on the <100 fs time scale
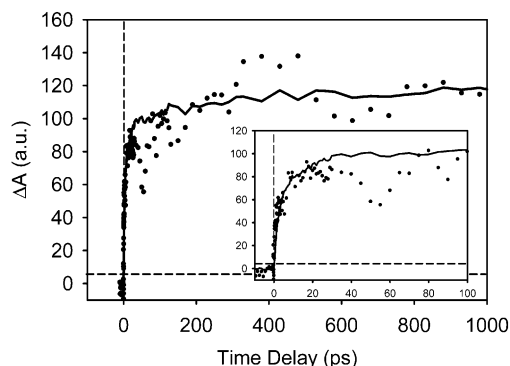
Figure 3. Comparison of electron signal (—) probed at 2120−2150 cm^{-1} and oxidized peak (●) dynamics for ReC1A/SnO$_2$ at pH 2. The oxidized peak dynamics were obtained by integrating the area between the actual signal and the underlying injected electron signal from 2086 to 2117 cm^{-1}, as discussed in the text. The inset shows earlier time comparison of the electron and oxidized signals. The traces show good agreement, indicating that either the electron or oxidized peak may be used to track electron injection into SnO$_2$.

and the electron signal was shown to exhibit substantial decay that was not mirrored by the ReC0A oxidized peak.[57,63] The decay was attributed to the relaxation of rapidly injected hot electrons in the semiconductor, leading to a decrease in their absorption cross section. Electron cross-section decay was not observed for ReC1/TiO$_2$, in which injection occurs on the 20 ps time scale.[57,63] In this case, the excited molecules relax to the ^{3}MLCT state and inject electrons near the band edge.

Kinetic traces for the oxidized peak and electron signal of ReC1A/SnO$_2$ are compared in Figure 3. The electron signal (solid line) is taken from the kinetic trace probing at 2120−2150 cm^{-1} to avoid contributions from dye vibrational modes. The oxidized peak kinetic trace is obtained by integrating the peak area from 2086 to 2117 cm^{-1} at each time delay. The size of the oxidized peak signal is then normalized for comparison with the electron signal and exhibits good agreement at all time delays, although the oxidized peak trace is comparatively noisy. We observed no evidence of electron cross-section decay for any of the complexes. This is consistent with the lack of a fast (<100 fs) injection component. Because cross-section decay is not significant, the electron signal may be employed to determine the bridge-length dependence of electron injection dynamics. This is strongly preferred in the present study because the oxidized peak is only 1−2% as intense as the electron signal, introducing noise to the oxidized peak trace. For TiO$_2$, we estimate that the absorption cross section of injected electrons is 8−10 times smaller than that in SnO$_2$, so use of the oxidized peak was not problematic in that case.

Dynamics of Charge Injection. The dependence of the electron signal on pump power was determined using excitation energies of 0.5−3.5 μJ/pulse at 400 nm. All obtained electron signal dynamics were identical within error, only varying in size. The signal sizes showed a linear dependence on pump power, indicating that the injection yield was unchanged. As a result, all transient absorption traces were collected using 2 μJ/pulse pump energy at 400 nm to ensure that electron injection results from single-photon excitation of the dye molecule.

Figure 4 shows injected electron traces probed at 2120−2150 cm^{-1} for the entire series of bridged rhenium dyes adsorbed on SnO$_2$ films at pH 2. In all cases, the background signal from unsensitized SnO$_2$ film (Figure 4) was subtracted to give the displayed traces. These traces were acquired with identical sample OD at 400 nm pump power and overlap between pump and probe beam. This allows quantitative comparison of relative
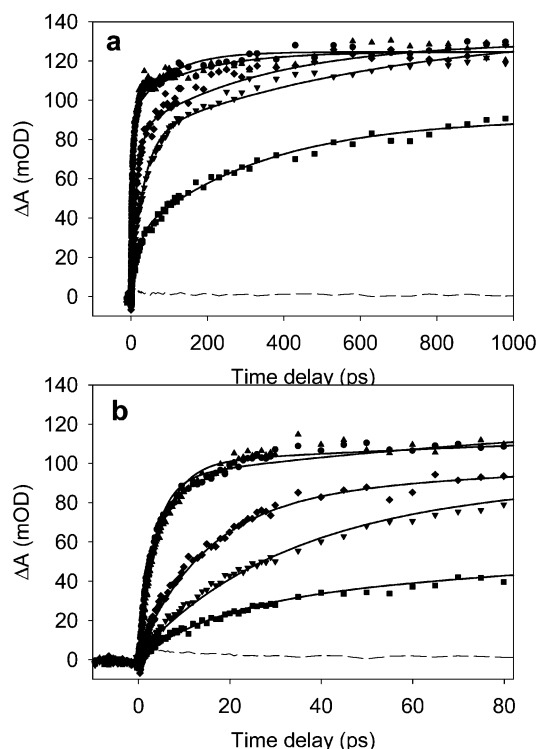

Figure 4. Injected electron traces probing at 2120−2150 cm^{-1} for ReC1A (●), ReC2A (▲), ReC3A (◆), ReC4A (▼), and ReC5A (■), all on SnO$_2$ film at pH 2. The lower frame expands the early-time dynamics. The solid lines are two-exponential fits to the data using the parameters of Table 1. The dashed line is the signal from an unsensitized SnO$_2$ film, which has been already been subtracted from the other traces.

signal sizes and thus the injection yield for different dyes. Film inhomogeneity and long-term laser instability introduced an estimated ±10% uncertainty to these relative signal intensities. At 1 ns, the signals observed for ReC1A, ReC2A, and ReC3A on SnO$_2$ have converged to similar values, suggesting that this signal size corresponds to complete injection, further supported by the virtually complete disappearance of the excited-state peak for ReC1A (Figure 2b) and the other sensitizers. Only the ReC5A/SnO$_2$ spectra exhibited the persistence of significant excited-state peak intensity at 1 ns, an observation consistent with its smaller and still-increasing electron signal. These results support the assumption that electron injection yield from these dyes does not vary with bridge length. This is quite reasonable because all dyes have similar excited-state energetics and their lifetimes are substantially longer than 1 ns. A previous study of ReC0A on ZrO$_2$ film, for which electron injection does not occur, showed that the dye excited-state lifetime was much greater than 1 ns.[63] Similar results were obtained for ReC1A, and the persistence of the bleach signal in Figure 2 provides additional evidence that non-ET decay pathways do not significantly affect electron injection kinetics within the 1 ns time window. The interruption of the conjugation between the bipyridine and the carboxylate groups by the methylene spacers renders the excited states electronically similar for compounds with $n > 1$ spacer units.

The electron traces in Figure 4 were fit using a convolution of the Gaussian instrument response function with a sum of two exponentials. These fits reasonably reproduce the injection dynamics, although there is noticeable error, particularly at intermediate times. This error likely indicates an inhomogeneous distribution of injection rates. Fitting parameters are shown in Table 1, in which the amplitudes are represented by A_1 and A_2

Bridge-Assisted Ultrafast Interfacial ET

J. Phys. Chem. B, Vol. 107, No. 51, 2003 **14235**

TABLE 1: Fitting Parameters for Injection Kinetics of ReC1A−ReC5A[a]

	τ_1, ps $(A_1, \%)$	τ_2, ps $(A_2, \%)$	τ_{eff} (ps)	τ_{eff} rel	$\langle\tau\rangle$ (ps)	$\langle\tau\rangle$ rel	τ_{scale}
ReC1A	3.8 (70)	128 (30)	41	1	41	1	1
ReC2A	4.8 (77)	175 (23)	44	1.1	45	1.1	1.00 ± 0.02
ReC3A	15 (62)	340 (38)	140	3.4	140	3.4	5.5 ± 0.5
ReC4A	32 (57)	640 (43)	290	7.1	230	5.6	13 ± 3
ReC5A	37 (30)	1300 (70)	950	23	500	12	40 ± 10

[a] Time scales and amplitudes for the two-exponential fits shown in Figure 4 are listed in columns 2 and 3. The values for τ_{eff} (column 4) are calculated as a weighted average of the two exponential time scales according to eq 2. $\langle\tau\rangle$ is calculated according to eq 3. Relative values are in relation to ReC1A in both cases. The time-scaling factors used to obtain Figure 5 and plotted in Figure 6 are listed in column 6. See discussion for the definition of the time-scaling factor, τ_{scale}.

and their corresponding time scales are τ_1 and τ_2. To facilitate quantitative comparison as a function of bridge length, the effective weighted time scales of injection, τ_{eff}, are calculated for each sensitizer as

$$\tau_{\text{eff}} = \frac{A_1\tau_1 + A_2\tau_2}{A_1 + A_2} \quad (2)$$

A more general means to express the effective time scale directly from the experimental data is[94]

$$\langle\tau\rangle = \int_0^\infty \frac{S(t) - S(\infty)}{S(0) - S(\infty)} \, dt \quad (3)$$

where $S(t)$ is the experimental signal size at time t. Values for $\langle\tau\rangle$ obtained by numerical integration of the data are shown in Table 1. For this calculation, integration was performed out to 1 ns. For $n = 1-3$, signal size at 1 ns is used as $S(\infty)$. Because the injection for ReC4A and ReC5A is clearly not complete at 1 ns, the values obtained only constitute lower limits for $\langle\tau\rangle$. We also assume that they approach the same $S(\infty)$ value as $n = 1-3$.

A comparison of τ_{eff} and $\langle\tau\rangle$ clearly demonstrates increasing injection time scale with bridge length. The only exceptions are ReC1A and ReC2A, the kinetic traces of which are virtually identical, giving very similar values for τ_{eff} and $\langle\tau\rangle$. However, quantitative use of the results obtained from either method is hindered by large uncertainty for longer bridges due to incomplete injection within the 1 ns time window. Incomplete injection leads to underestimate of the contribution of the slow component to $\langle\tau\rangle$. With the use of two-exponential fit, the time-constant for the slow component is poorly determined for $n = 4$ and 5, which results in uncertainty in τ_{eff}. Therefore, an alternative approach for determining relative injection rate as a function of bridge length will be developed to allow clear quantitative analysis of the experimental results.

Discussion

Determination of Quantitative Differences in Injection Rate. The results presented above clearly indicate a rate decrease with longer methylene bridges between the bipyridene ligand and the carboxylate anchoring groups. However, electron injection is nonexponential, complicating quantitative analysis. Nonexponential electron injection dynamics have been previously observed in Ru dye-sensitized TiO$_2$ thin films.[31,61,69,70,75] In these films, injection dynamics are biphasic, consisting of a fast component (attributed to injection from unthermalized excited state) and non-single-exponential slower components

(ascribed to injection from the thermalized excited state in a distribution of local environments/orientations). We have shown in many other dye-sensitized nanocrystalline thin films, such as ReC*n* on TiO$_2$,[57] Ru dyes on SnO$_2$,[66] and Ru N3 on ZnO,[61] that non-single-exponential injection kinetics are a common feature of interfacial electron transfer whenever they are slow enough to be clearly resolved. The inhomogeneous distribution of interfacial ET was clearly shown in an elegant single-molecule electron-transfer study.[95]

The bridged dyes presented here exhibit no fast injection component. Insertion of a nonconjugated bridge slows electron injection, resulting in dominance of intramolecular relaxation processes over injection from unthermalized excited state. Virtually all injection from the bridged sensitizers occurs from the fully relaxed excited state. In the weak coupling limit, the total ET rate for this system may be expressed as the sum of ET rates to all possible accepting states in the semiconductor. Adopting an approach similar to that of Marcus and co-workers,[66,96−98] we may express the total ET rate from adsorbate to semiconductor:

$$k_{\text{ET}} = \frac{2\pi}{h} \int_{-\infty}^{\infty} dE \, \rho(E) |\bar{H}(E)|^2 \frac{1}{\sqrt{4\pi\lambda k_{\text{B}}T}} \times$$
$$\exp\left[-\frac{(\lambda + \Delta G_0 - E)^2}{4\lambda k_{\text{B}}T}\right] \quad (4)$$

In eq 4, $\Delta G_0 = E_{\text{CB}} - E_{\text{ox}}$ is the energy difference between conduction band edge and the redox potential of adsorbate excited state; $\rho(E)$ is the density of semiconductor states at energy E from the conduction band edge; $H(E)$ is the average electronic coupling between the adsorbate excited state and different **k** states in the semiconductor at the same energy E; λ is the total reorganization energy.

However, as noted above, a distribution of adsorbate/semiconductor interactions exists, implying a distribution of injection rates. The total population of injected electrons, $N_{\text{e}}(t)$, may then be given by integrating eq 4 over the distribution function:

$$N_{\text{e}}(t) = N_0[1 - \int_{-\infty}^{\infty} g(\theta) \, e^{-k(\theta)t} \, d\theta] \quad (5)$$

In eq 5, N_0 is the total number of excited molecules and the normalized distribution of adsorbate is represented by $g(\theta)$, where θ incorporates all parameters that can affect the injection rate, $k(\theta)$. According to eq 4, the rate is affected by the electronic coupling strength, reorganization energy, adsorbate redox potential, density of states, and semiconductor conduction band edge. Heterogeneous distributions of these quantities can arise from variations of adsorbate/semiconductor binding geometry, adsorbate conformation, the local interfacial environment of binding site, crystal faces, and defects. Still, using eq 5 to directly fit the kinetic traces is problematic because $g(\theta)$ is not well established. However, this equation suggests a method by which the relative injection rate of different bridge length may be compared quantitatively without defining $g(\theta)$.

Consider two samples of different bridge length, n and n', with distributions $g_n(\theta)$ and $g_{n'}(\theta)$ and injection rates $k_n(\theta)$ and $k_{n'}(\theta)$. In the special case where $g_n(\theta) = g_{n'}(\theta)$, and $k_n(\theta) = Ck_{n'}(\theta)$, the relative injection rate C can be obtained without fitting the data or knowing the distribution function, $g_n(\theta)$. For
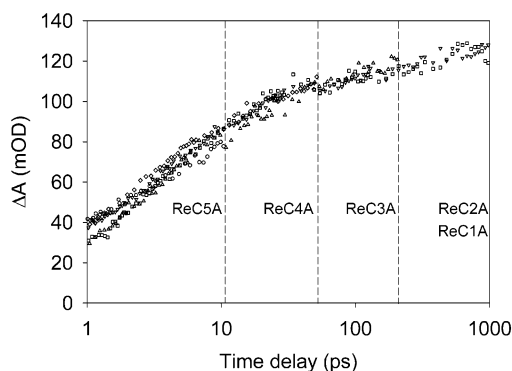
14236 *J. Phys. Chem. B, Vol. 107, No. 51, 2003*

Anderson et al.

Figure 5. Injected electron traces for ReC1A–ReC5A on SnO_2 after applying the time-scaling technique described in the text. ReC1A is represented by the downward-pointing triangles, ReC2A by squares, ReC3A by upward-pointing triangles, ReC4A by diamonds, and ReC5A by circles. All traces extended to 1 ns delay prior to scaling. Therefore, the ratio between 1 ns and the ending time of each trace (shown by the vertical lines) corresponds to the time-scale factor used. Very good agreement among all traces is obtained, except very early in the injection, when longer-bridged dyes inject slightly faster than shorter-bridged dyes. This agreement allows quantitative comparison of the relative rates, as determined from the time-scaling factors.

the case described above,

$$N_{n'}(t) = N_0[1 - \int_{-\infty}^{\infty} g_{n'}(\theta)\, e^{-K_{n'}(\theta)t}\, d\theta] =$$

$$N_0[1 - \int_{-\infty}^{\infty} g_n(\theta)\, e^{-K_n(\theta)t/C}\, d\theta] \rightarrow$$

$$N_n(t') = N_{n'}(t/C) = N_n(t) \quad (6)$$

Therefore, a difference in rate may be transformed into a difference in the time parameters of the kinetic traces. Scaling the time parameters of the kinetics trace for bridge n' sample by a $1/C$ factor will cause it to match the trace for bridge n. The time-scaling factor C is exactly the relative ratio of the electron-transfer rates between the two samples and can be quantitatively obtained without knowing the distribution function.

The results from applying the time-scaling technique to all samples from ReC1A to ReC5A on SnO_2 are shown in Figure 5. In employing this approach, we used the kinetic traces from Figure 4, which correspond to identical experimental conditions for all dyes. ReC1A/SnO_2 was used as a standard to which subsequent samples were matched. The time-scaling factor is the only free parameter in this fitting technique. A size-scaling factor was introduced as a constrained parameter for each trace and allowed to vary from 0.9 to 1.1 to achieve the best fit. This permits correction for the estimated 10% uncertainty in signal sizes arising from sample heterogeneity and long-term laser instability. The time-scaling technique results in excellent agreement between the traces except for some deviation very early in the injection process. The time-scaling parameters used to obtain Figure 5 are listed in Table 1. The error bars reflect the range of time and signal size scaling factors that result in a satisfactory fit to the ReC1A trace.

Justification of the Time-Scaling Approach. The major assumptions implicit in applying eq 6 are that the distribution function $g(\theta)$ is independent of bridge length and the rate constants for different bridge lengths differ by a simple factor. This technique is not likely to be suitable for comparing disparate samples with different basic structures. However, the present investigation uses molecules with very similar chromophores and the same binding group. The salient issue is whether the distribution is reasonably independent of methylene

bridge length. Other than the obvious electronic coupling factor, it is important to address whether other ET rate-determining parameters may also be affected by bridge length. As shown by eq 4, these factors include reorganization energy, density of states in the semiconductor, and relative energetics of the adsorbate and semiconductor.

The flexibility of the methylene bridges may lead to conformational distributions and therefore coupling strength distributions that vary with bridge length. Interestingly, the effect of conformational distribution is noted in some studies[52] but not others.[56] One study of donor–methylene bridge–acceptor molecular complexes demonstrated that the bridge conformation has relatively little effect on electron-transfer rate for $n < 5$ but that the effect is noticeable with longer spacer units.[56] In contrast, the possible influence of bridge conformation on ET rate has been suggested in other bridged donor–acceptor systems for short bridge lengths.[52] The other primary factor in the coupling distribution is the local binding environments on the surface. However, local binding depends primarily upon interactions between carboxylate groups and the semiconductor, so bridge-length dependence is not anticipated.

Some distance dependence of the reorganization energy (λ) is possible but predicted to be shallow for semiconductors because of an attenuated image charge response in the semiconductor.[99] Additionally, all experiments were performed on the same batch of SnO_2 films, and the injection kinetics of each adsorbate on different films were reproducible within experimental signal-to-noise ratios. Therefore, it is reasonable to assume that all films have similar distributions of exposed crystal faces, trap state densities, and surface environments for adsorbate binding.

The applicability of the time-scaling technique for this series of compounds implies a distribution function $g(\theta)$ that is relatively invariant with bridge length. Most likely, this uniformity indicates that the distribution function is determined primarily by the interfacial binding environment of each molecule to the semiconductor. Thus, bridge-length-dependent effects, such as bridge conformation and reorganization energy, apparently have a smaller effect in these systems.

Bridge-Length Dependence of Electron Injection. Because of the excellent agreement among all of the time-scaled traces, it is appropriate to use time-scaling in ascertaining relative injection rates as a function of bridge length. The rates so obtained are superior to τ_{eff} and $\langle\tau\rangle$ from Table 1 because the latter values are more sensitive to ongoing injection beyond the time window. The injection rate as a function of bridge length is plotted in Figure 6. The data points therein are determined by multiplying each relative injection rate from time scaling by $\langle\tau\rangle_{(ReC1A)} = 41$ ps. ReC1A and ReC2A exhibit nearly identical rates, while ReC3A, ReC4A, and ReC5A show rates decreasing exponentially with bridge length, as predicted by eq 1. A linear regression analysis of these data gives a value of $\beta_n = 1.0$, regardless of whether ReC1A and ReC2A are included in the fit. Using an average distance increase of 1.27 Å per CH_2 unit in an all-anti alkyl chain,[46] the decay coefficient in terms of distance is $\beta_r = 0.79$ Å^{-1}.

The β_n value determined for this system is agreement with $\beta_n = 1.0-1.2$ obtained for alkanethiols ($n > 8$) on Au electrodes.[11,12,16,18,19,41,42,100] This value, however, is quite different from $\beta_n = 0.5$ ($n = 8-16$) for alkanethiols on InP electrodes.[14,15] The agreement with the longer alkyl chain on Au may be fortuitous because of the different bridge-length dependence of reorganization energy on different electrodes and at different chain lengths (due to image charge). Solvent
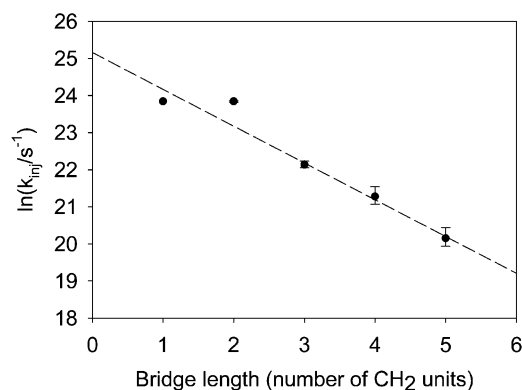
Bridge-Assisted Ultrafast Interfacial ET

J. Phys. Chem. B, Vol. 107, No. 51, 2003 **14237**

Figure 6. Plot of the logarithm of injection rate versus number of methylene bridging groups. The relative rates (with respect to ReC1A/SnO2) were determined using the time-scaling technique described in the text. The absolute rate was then obtained by multiplying these scaling factors by the ReC1A $\tau_{eff} = 44$ ps determined in Table 1. ReC1A and ReC2A exhibited nearly identical rates, but ReC3A−ReC5A show a linear trend with $\beta_n = 0.99$.

reorganization energy increases more rapidly with chain length on metal electrodes compared to semiconductor and at short chain length ($n = 1-5$) compared to longer ones.[99] For alkanethiol-modified Au electrodes, the corrections to the β_r value are estimated to be $\beta_r = 0.08$ Å^{-1} for $n = 5-10$ and $\beta_r < 0.04$ Å^{-1} for longer chains. Using the dielectric continuum model[101] (with static and optical dielectric constants of 13 and 4 for SnO$_2$ and 78 and 1.78 for water and spherical cavity radius of 6.8 Å for Re complexes), we estimated that going from ReC1A to ReC5A on a SnO$_2$/water interface resulted in only a 0.03 eV change in reorganization energy, which has a negligible effect on the ET rate.

The $\beta_r = 0.79$ Å^{-1} value determined for this system falls in the range of β_r values (0.5−0.9 Å^{-1}) calculated for electron transfer through saturated alkane chains via the superexchange model.[43,46−49,102] Larger β_r values (~3 Å^{-1}) are expected for a through-space ET pathway.[102] This suggests an important role of the methylene bridge in assisting electron injection from Re complex to SnO$_2$ nanocrystalline thin films.

An interesting feature of Figure 6 is the departure from linearity for ReC1A and ReC2A. Two possible explanations have been suggested for this deviation at very short bridge length. One is a breakdown in the exponential dependence of electronic coupling on spacer length in this regime,[43,46−49,102] an effect that has been predicted by theoretical calculations that estimate anion coupling as a function of methylene bridge length.[43,46−49,102] These computational studies indicate an exponential dependence of coupling on bridge length for all cases except $n = 1$ or 2, in which the coupling falls substantially below the exponential trend. The present experiments may be the first experimental demonstration of this type of breakdown.

Another possible explanation for the deviation at short bridge length was proposed in a recent study of Fe(II)(CN)$_6^{4-}$/Fe(III)(CN)$_6^{3-}$ on short-chain alkanethiol ($n = 2-8$) modified Au electrodes.[23] An exponential dependence of ET rate with $\beta_r = 1.04$ Å^{-1} was observed for $n = 4-8$, but a smaller β value was observed for $n < 4$. Furthermore, the ET rate for $n = 2$ was found to be dependent on solvent viscosity. The proposed explanation for this behavior was that at $n = 2$ and bare Au electrode, the ET process may fall into the adiabatic regime, in which the solvent relaxation time may dictate the ET rate. However, in our system, the effective ET times for $n = 1$ and 2 are still on the time scale of tens of picoseconds. It is unclear whether this process is too slow to be limited by solvent

relaxation time. Solvent relaxation time for bulk water has a substantial subpicosecond component.[103] A recent study of solvation dynamics at a ZrO$_2$/aqueous water interface demonstrated a slightly faster solvation time compared to bulk water.[104,105] Not enough data yet exist to elucidate the reasons for the departure from linearity. Certainly, this deviation merits further study to provide more complete understanding of electron transfer through very short bridges. Therefore, ongoing experiments will examine not only the solvent dependence at short bridge length but also the effects of bridge length on other semiconductors. It should be noted that departure from exponential dependence has been observed for interfacial ET at even longer distance for alkanethiol ($n = 5-8$)[12,40] and oligophenylenevinylene bridges[22] using the indirect laser-induced temperature jump technique. Although it is still not understood, this behavior appears to be independent of the identity of redox couple and the nature of the linkage of the couple to the bridge.[12,40] It is therefore also informative to extend our study to longer spacer units and longer time window.

Summary

In conclusion, a systematic and quantitative investigation of the relative rates of photoinduced interfacial electron transfer as a function of methylene bridge length in the short-bridge limit has been accomplished. A novel time-scaling technique to compare kinetic traces allowed the comparison of the nonexponential injection times. For all bridged samples ($n = 1-5$), the application of this method indicated a distribution of ET rates that was nominally independent of bridge length. The results exhibited an exponential dependence of the rate on bridge length for $n = 3-5$ methylene units with $\beta_n = 1.0$, a value consistent with results obtained previously for electron transfer through longer bridges. The breakdown of this exponential dependence for $n = 1$ and 2 is interesting and may indicate a leveling of electronic coupling at short bridge length, as predicted by prior theoretical studies.

Supporting Information Available: Detailed synthetic procedures and spectroscopic data for the Re(CO)$_3$Cl complexes **1a−e** and **3a−e**. These materials are available free of charge via the Internet at http://pubs.acs.org.

References and Notes

(1) Closs, G. L.; Miller, J. R. *Science* **1988**, *240*, 440.
(2) Moser, C. C.; Keske, J. M.; Warncke, K.; Farid, R. S.; Dutton, P. L. *Nature* **1992**, *355*, 796.
(3) Mayo, S. L.; Ellis, W. R.; Crutchley, R. J.; Gray, H. R. *Science* **1986**, *233*, 948.
(4) Arkin, M. R.; Stemp, E. D. A.; Holmlin, R. E.; Barton, J. K.; Hormann, A.; Olson, E. J. C.; Barbara, P. F. *Science* **1996**, *273*, 475.
(5) Berlin, Y. A.; Burin, A. L.; Ratner, M. A. *J. Am. Chem. Soc.* **2001**, *123*, 260.
(6) Aviram, A.; Ratner, M. A. *Chem. Phys. Lett.* **1974**, *29*, 277.
(7) Nitzan, A. *Annu. Rev. Phys. Chem.* **2001**, *52*, 681.
(8) Pease, A. R.; Jeppesen, J. O.; Stoddart, J. F.; Luo, Y.; Collier, C. P.; Heath, J. R. *Acc. Chem. Res.* **2001**, *34*, 433.

(9) Chen, J.; Reed, M. A.; Rawlett, A. M.; Tour, J. M. *Science* **1999**, *286*, 1550.

(10) Cui, X. D.; Primak, A.; Zarate, X.; Tomfohr, J.; Sankey, O. F.; Moore, A. L.; Moore, T. A.; Gust, D.; Harris, G.; Lindsay, S. M. *Science* **2001**, *294*, 571.

(11) Chidsey, C. E. D. *Science* **1991**, *251*, 919.

(12) Smalley, J. F.; Feldberg, S. W.; Chidsey, C. E. D.; Linford, M. R.; Newton, M. D.; Liu, Y. P. *J. Phys. Chem.* **1995**, *99*, 13141.

(13) Sachs, S. B.; Dudek, S. P.; Hsung, R. P.; Sita, L. R.; Smalley, J. F.; Newton, M. D.; Feldberg, S. W.; Chidsey, C. E. D. *J. Am. Chem. Soc.* **1997**, *119*, 10563.

(14) Gu, Y.; Waldeck, D. H. *J. Phys. Chem. B* **1998**, *102*, 9015.

(15) Gu, Y.; Waldeck, D. H. *J. Phys. Chem.* **1996**, *100*, 9573.

(16) Guo, L.-H.; Facci, J. S.; McLendon, G. *J. Phys. Chem.* **1995**, *99*, 8458.

(17) Miller, C.; Gratzel, M. *J. Phys. Chem.* **1991**, *95*, 5225.

(18) Becka, A. M.; Miller, C. J. *J. Phys. Chem.* **1992**, *96*, 2657.

(19) Finklea, H. O.; Hanshew, D. D. *J. Am. Chem. Soc.* **1992**, *114*, 3173.

(20) Creager, S.; Yu, C. J.; Bamdad, C.; O'Connor, S.; MaLean, T.; Lam, E.; Chong, Y.; Olsen, G. T.; Luo, J.; Gozin, M.; Kayyem, J. F. *J. Am. Chem. Soc.* **1999**, *121*, 1059.

(21) Weber, K. S.; Creager, S. E. *J. Electroanal. Chem.* **1998**, *458*, 17.

(22) Sikes, H. D.; Smalley, J. F.; Dudek, S. P.; Cook, A. R.; Newton, M. D.; Chidsey, C. E. D.; Feldberg, S. W. *Science* **2001**, *291*, 1519.

(23) Khoshtariya, D. E.; Dolidze, T. D.; Zusman, L. D.; Waldeck, D. H. *J. Phys. Chem. A* **2001**, *105*, 1818.

(24) Li, T. T.-T.; Weaver, M. J. *J. Am. Chem. Soc.* **1984**, *106*, 6107.

(25) Bach, U.; Lupo, D.; Comte, P.; Moser, J. E.; Weissortel, F.; Salbeck, J.; Spreitzer, H.; Gratzel, M. *Nature* **1998**, *395*, 583.

(26) Nazeeruddin, M. K.; Kay, A.; Rodicio, I.; Humphrybaker, R.; Muller, E.; Liska, P.; Vlachopoulos, N.; Gratzel, M. *J. Am. Chem. Soc.* **1993**, *115*, 6382.

(27) O'Regan, B.; Gratzel, M. *Nature* **1991**, *353*, 737.

(28) Tachibana, Y.; Moser, J. E.; Graetzel, M.; Klug, D. R.; Durrant, J. R. *J. Phys. Chem.* **1996**, *100*, 20056.

(29) Asbury, J. B.; Ellingson, R. J.; Ghosh, H. N.; Ferrere, S.; Nozik, A. J.; Lian, T. *J. Phys. Chem. B* **1999**, *103*, 3110.

(30) Hannappel, T.; Burfeindt, B.; Storck, W.; Willig, F. *J. Phys. Chem. B* **1997**, *101*, 6799.

(31) Banko, G.; Kalloinen, J.; Korppi-Tommola, J. E. I.; Yartsev, A. P.; Sundstrom, V. *J. Am. Chem. Soc.* **2002**, *124*, 489.

(32) Haque, S. A.; Tachibana, Y.; Klug, D. R.; Durrant, J. R. *J. Phys. Chem. B* **1998**, *102*, 1745.

(33) Haque, S. A.; Tachibana, Y.; Willis, R. L.; Moser, J. E.; Graetzel, M.; Klug, D. R.; Durrant, J. R. *J. Phys. Chem. B* **2000**, *104*, 538.

(34) Piotrowiak, P.; Galoppini, E.; Guo, W.; Wei, Q.; Meyer, G. J.; Woewior, P. *J. Am. Chem. Soc.* **2003**, *125*, 5278.

(35) Hoertz, P. G.; Carlisle, R. A.; Meyer, G. J.; Wang, D.; Piotrowiak, P.; Galoppini, E. *Nano Lett.* **2003**, *3*, 325.

(36) Galoppini, E.; Guo, W.; Zhang, W.; Hoertz, P. G.; Qu, P.; Meyer, G. J. *J. Am. Chem. Soc.* **2002**, *124*, 7801.

(37) Galoppini, E.; Guo, W.; Qu, P.; Meyer, G. J. *J. Am. Chem. Soc.* **2001**, *123*, 4342.

(38) Kilsa, K.; Mayo, E. I.; Kuciauskas, D.; Villahermosa, R.; Lewis, N. S.; Winkler, J. R.; Gray, H. B. *J. Phys. Chem. A* **2003**, *107*, 3379.

(39) Yaliraki, S. M. K., M.; Ratner, M. A. *J. Am. Chem. Soc.* **1999**, *121*, 3428.

(40) Smalley, J. F.; Finklea, H. O.; Chidsey, C. E. D.; Linford, M. R.; Creager, S. E.; Ferraris, J. P.; Chalfant, K.; Zawodzinsk, T.; Feldberg, S. W.; Newton, M. D. *J. Am. Chem. Soc.* **2003**, *125*, 2004.

(41) Carter, M. T.; Rowe, G. K.; Richardson, J. N.; Tender, L. M.; Terrill, R. H.; Murray, R. W. *J. Am. Chem. Soc.* **1995**, *117*, 2896.

(42) Rowe, G. K.; Carter, M. T.; Richardson, J. N.; Murray, R. W. *Langmuir* **1995**, *11*, 1797.

(43) Newton, M. D. *Chem. Rev.* **1991**, *91*, 767.

(44) Jordan, K. D.; Paddon-Row, M. N. *Chem. Rev.* **1992**, *92*, 395.

(45) McConnell, H. M. *J. Chem. Phys.* **1961**, *35*, 508.

(46) Liang, C. X.; Newton, M. D. *J. Phys. Chem.* **1993**, *97*, 3199.

(47) Liang, C. X.; Newton, M. D. *J. Phys. Chem.* **1992**, *96*, 2855.

(48) Curtiss, L. A.; Miller, J. R. *J. Phys. Chem. A* **1998**, *102*, 160.

(49) Curtiss, L. A.; Naleway, C. A.; Miller, J. R. *J. Phys. Chem.* **1993**, *97*, 4059.

(50) Hsu, C.-P. *J. Electroanal. Chem.* **1997**, *438*, 27.

(51) Hsu, C.-P.; Marcus, R. A. *J. Chem. Phys.* **1997**, *106*, 584.

(52) Ryu, C. K.; Wang, R.; Schmehl, R. H.; Ferrere, S.; Ludwikow, M.; Merkert, J. W.; Headford, C. E. L.; Elliott, C. M. *J. Am. Chem. Soc.* **1992**, *114*, 430.

(53) Schanze, K. S.; Walters, K. A. Photoinduced Electron Transfer in Metal-Organic Dyads. In *Organic and Inorganic Photochemistry*; Schanze, K. S., Ed.; Marcel-Dekker: New York, 1998; Vol. 2, p 75.

(54) Larson, S. L.; Elliott, C. M.; Kelley, D. F. *J. Phys. Chem.* **1995**, *99*, 6530.

(55) Yonemoto, E. H.; Kim, Y. I.; Schmehl, R. H.; Wallin, J. O.; Shoulders, B. A.; Richardson, B. R.; Haw, J. F.; Mallouk, T. E. *J. Am. Chem. Soc.* **1994**, *116*, 10557.

(56) Yonemoto, E. H.; Saupe, G. B.; Schmehl, R. H.; Hubig, S. M.; Riley, R. L.; Iverson, B. L.; Mallouk, T. E. *J. Am. Chem. Soc.* **1994**, *116*, 4786.

(57) Asbury, J. B.; Hao, E.; Wang, Y.; Lian, T. *J. Phys. Chem. B* **2000**, *104*, 11957.

(58) Ramakrishna, S.; Willig, F.; May, V. *Chem. Phys. Lett.* **2002**, *351*, 242.

(59) Huber, R.; Moser, J. E.; Gratzel, M.; Wachtveitl, J. *J. Phys. Chem. B* **2002**, *106*, 6494.

(60) Ellingson, R. J.; Asbury, J. B.; Ferrere, S.; Ghosh, H. N.; Sprague, J. R.; Lian, T.; Nozik, A. J. *J. Phys. Chem. B* **1998**, *102*, 6455.

(61) Asbury, J. B.; Wang, Y.; Lian, T. *J. Phys. Chem. B* **1999**, *103*, 6643.

(62) Ghosh, H. N.; Asbury, J. B.; Lian, T. *PINSA-A: Proc. Indian Natl. Sci. Acad., Part A* **2000**, *66*, 177.

(63) Wang, Y.; Asbury, J. B.; Lian, T. *J. Phys. Chem. A* **2000**, *104*, 4291.

(64) Anderson, N. A.; Hao, E.; Ai, X.; Hastings, G.; Lian, T. *Chem. Phys. Lett.* **2001**, *347*, 304.

(65) Asbury, J. B.; Wang, Y. Q.; Hao, E. C.; Ghosh, H. N.; Lian, T. *Res. Chem. Int.* **2001**, *27*, 315.

(66) Asbury, J. B.; Hao, E.; Wang, Y.; Ghosh, H. N.; Lian, T. *J. Phys. Chem. B* **2001**, *105*, 4545.

(67) Hao, E.; Anderson, N. A.; Asbury, J. B.; Lian, T. *J. Phys. Chem. B* **2002**, *106*, 10191.

(68) Tachibana, Y.; Haque, S. A.; Mercer, I. P.; Moser, J. E.; Klug, D. R.; Durrant, J. R. *J. Phys. Chem. B* **2001**, *105*, 7424.

(69) Tachibana, Y.; Haque, S. A.; Mercer, I. P.; Durrant, J. R.; Klug, D. R. *J. Phys. Chem. B* **2000**, *104*, 1198.

(70) Durrant, J. R.; Tachibana, Y.; Mercer, I.; Moser, J. E.; Gratzel, M.; Klug, D. R. *Z. Phys. Chem.* **1999**, *212*, 93.

(71) Bach, U.; Tachibana, Y.; Moser, J.-E.; Haque, S. A.; Durrant, J. R.; Graetzel, M.; Klug, D. R. *J. Am. Chem. Soc.* **1999**, *121*, 7445.

(72) Zimmermann, C.; Eichberger, R.; Ramakrishna, S.; Storck, W.; Willig, F. Photoinduced heterogeneous electron-transfer modulated by a vibrational wave packet. In *Femtochemistry and Femtobiology: Ultrafast Dynamics in Molecular Science*, Toledo, Spain, September 2−6, 2001; 2002.

(73) Ramakrishna, S.; Willig, F.; May, V. *Phys. Rev. B* **2000**, *62*, R16330.

(74) Burfeindt, B.; Zimmermann, C.; Ramakrishna, S.; Hannappel, T.; Meissner, B.; Storck, W.; Willig, F. *Z. Phys. Chem. (Muenchen)* **1999**, *212*, 67.

(75) Kalloinen, J.; Banko, G.; Sundstrom, V.; Korppi-Tommola, J. E. I.; Yartsev, A. P. *J. Phys. Chem. B* **2002**, *106*, 4396.

(76) Kuciauskas, D.; Monat, J. E.; Villahermosa, R.; Gray, H. B.; Lewis, N. S.; McCusker, J. K. *J. Phys. Chem. B* **2002**, *106*, 9347.

(77) Kuciauskas, D.; Freund, M.; Winkler, J. R.; Gray, H. B.; Lewis, N. S. *Proc.−Electrochem. Soc.* **2001**, *2001-10*, 125.

(78) Heimer, T.; Heilweil, E. J. *J. Phys. Chem. B* **1997**, *101*, 10990.

(79) Heimer, T. A.; D'Arcangelis, S. T.; Farzad, F.; Stipkala, J. M.; Meyer, G. J. *Inorg. Chem.* **1996**, *35*, 5319.

(80) Bauer, C.; Boschloo, G.; Mukhtar, E.; Hagfeldt, A. *J. Phys. Chem. B* **2001**, *105*, 5585.

(81) Ghosh, H. N.; Asbury, J. B.; Lian, T. *J. Phys. Chem. B* **1998**, *102*, 6482.

(82) Ghosh, H. N.; Asbury, J. B.; Weng, Y.; Lian, T. *J. Phys. Chem. B* **1998**, *102*, 10208.

(83) Hagfeldt, A.; Gratzel, M. *Chem. Rev.* **1995**, *95*, 49.

(84) Worl, L. A.; Duesing, R.; Chen, P.; Ciana, L. D.; Meyer, T. J. *J. Chem. Soc., Dalton Trans.* **1991**, 849.

(85) Wrighton, M.; Morse, D. L. *J. Am. Chem. Soc.* **1974**, *96*, 998.

(86) Hasselmann, G. M.; Meyer, G. J. *J. Phys. Chem. B* **1999**, *103*, 7671.

(87) Mohler, D. L.; Chen, D.; Reddy, V. B. *Synthesis* **2002**, 745.

(88) Costa, I.; Montalti, M.; Pallavicini, P.; Perotti, A.; Prodi, L.; Zaccheroni, N. *J. Organomet. Chem.* **2000**, *593−594*, 267.

(89) Nutz, T.; Felde, U. Z.; Haase, M. *J. Chem. Phys.* **1999**, *110*, 12142.

(90) George, M. W.; Turner, J. J. *Coord. Chem. Rev.* **1998**, *177*, 201.

(91) Turner, J. J.; George, M. W.; Johnson, F. P. A.; Westwell, J. R. *Coord. Chem. Rev.* **1993**, *125*, 101.

(92) Gamelin, D. R.; George, M. W.; Glyn, P.; Grevels, F. W.; Johnson, F. P. A.; Klotzbucher, W.; Morrison, S. L.; Russell, G.; Schaffner, K.; Turner, J. J. *Inorg. Chem.* **1994**, *33*, 3246.

(93) Clark, I. P.; George, M. W.; Johnson, F. P. A.; Turner, J. J. *Chem. Commun. (Cambridge)* **1996**, 1587.

(94) Maroncelli, M.; Fleming, G. R. *J. Chem. Phys.* **1987**, *86*, 6221.

(95) Lu, H. P.; Xie, X. S. *J. Phys. Chem. B* **1997**, *101*, 2753.

(96) Gao, Y. Q.; Georgievskii, Y.; Marcus, R. A. *J. Chem. Phys.* **2000**, *112*, 3358.

(97) Gao, Y. Q.; Marcus, R. A. *J. Chem. Phys.* **2000**, *113*, 6351.

Bridge-Assisted Ultrafast Interfacial ET

J. Phys. Chem. B, Vol. 107, No. 51, 2003 **14239**

(98) Gosavi, S.; Marcus, R. A. *J. Phys. Chem. B* **2000**, *104*, 2067.

(99) Liu, Y. P.; Newton, M. D. *J. Phys. Chem.* **1994**, *98*, 7162.

(100) Weber, K.; Hockett, L.; Creager, S. *J. Phys. Chem. B* **1997**, *101*, 8286.

(101) Marcus, R. A. *J. Phys. Chem.* **1990**, *94*, 1050.

(102) Curtiss, L. A.; Naleway, C. A.; Miller, J. R. *Chem. Phys.* **1993**, *176*, 387.

(103) Maroncelli, M.; Fleming, G. R. *J. Chem. Phys.* **1988**, *88*, 5044.

(104) Pant, D.; Levinger, N. E. *J. Phys. Chem. B* **1999**, *103*, 7846.

(105) Pant, D.; Levinger, N. E. *Chem. Phys. Lett.* **1998**, *292*, 200.